A Simple Model of Millennial Oscillations of the Thermohaline Circulation

A. COLIN DE VERDIÈRE

Laboratoire de Physique des Océans, Brest, France

(Manuscript received 8 February 2006, in final form 3 August 2006)

ABSTRACT

Stommel's two-box model of thermohaline circulation is modified to include the possibility of convection. When reduced to a two-degrees-of-freedom dynamical system, the model exhibits the well-known multiple (thermal and haline) steady states as well as new convective thermal steady states. However, for some values of the control parameters (such as the freshwater flux) oscillations occur. Millennial period oscillatory regimes correspond to switches between the Stommel's haline fixed point and the convective thermal state, both of which are unstable in a window of precipitation values. The transitions between steady and oscillatory regimes at the boundaries of the window are global bifurcations, which in some cases have an infinite period character. This character is due either to the proximity of the Stommel saddle node bifurcation or to the infinite time it takes for the convection to resume when the system is in the haline regime. The oscillations bear a close relationship to those of Welander's flip–flop model. The physics of this class of millennial oscillations may be relevant to those observed in more complex OGCMs and may help to rationalize certain features of the millennial band oscillations that punctuate the last glacial period.

1. Introduction

Oscillations in OGCMs under mixed surface boundary conditions (restoring on surface temperature, imposed freshwater flux) have now been widely reported and are found to occur in several frequency bands: decadal, centennial, millennial [see the reviews by Weaver and Hughes (1992) and Dijkstra and Ghil (2005)]. A strong incentive for a better understanding of the oscillations of the thermohaline circulation (THC) comes from the paleoclimatic evidence originating from ice cores and marine sediments that millennial band oscillations have punctuated the last glacial period (Alley et al. 1999). It is widely believed that variations of the thermohaline circulation of the North Atlantic Ocean are involved in the very existence of these oscillations (Broecker et al. 1990). Yet to be found, however, is a generally accepted picture of their physics. Stommel's (1961) two-box model has provided the leading ideas to show the possibility of two stable regimes of THC under mixed boundary conditions. Since the model does not oscillate (Ruddick and Zhang 1996), many authors have used time-dependent forcings to produce oscillations. Indeed one of the current explanations of the Dansgaard–Oeschger millennial events of the last glacial maximum is the so-called stochastic resonance mechanism, which combines periodic forcing and noise to produce transitions between stable regimes of flow (Alley et al. 2001; Velez-Belchi et al. 2001; Ganopolski and Rahmstorf 2002). Munk and Dzieciuch (2002) have drawn attention to the difficulties for nonlinear processes to close the 10-octave gap between tidal and Milankowitch forcings and generate millennial external forcing. The existence of self-sustained thermohaline oscillations in a (vertical) water column was demonstrated by Welander (1982). Although oscillations were known to exist in double-diffusive convection (Turner 1973), Welander was looking for oscillations that depended, instead, on the different surface boundary conditions for temperature and salinity. His model consists of a single active box connected to an upper reservoir of given temperature–salinity values (kept constant by other processes) with different surface exchange time scales for temperature and salinity and to a lower reservoir (deep water) whose exchange is diffusive (weak) if the stratification is stable or convective (strong) otherwise. Such a model oscillates when the upper reservoir is warmer and saltier than the lower reservoir.

Corresponding author address: Alain Colin de Verdière, Université de Bretagne Occidentale, Laboratoire de Physique des Océans, 6 Ave. Le Gorgeu, C.S. 93837, 29238 Brest CEDEX 3, France.
E-mail: acolindv@univ-brest.fr

DOI: 10.1175/JPO3056.1

Cessi (1996) pursued Welander's analysis and identified several characteristics of the Welander model shared by interdecadal oscillations found in OGCMs. However, this model cannot describe oscillations of the circulation per se since advective processes are neglected altogether. Therefore we have on the one hand a circulation model with multiple steady states only and on the other hand a model of oscillatory convection without circulation. Finding a model amenable to theoretical analysis that includes *both circulation* and *convection* of the THC is certainly an appealing idea. With this goal in mind, Huang et al. (1992) constructed 2×2 and 3×2 box models but no oscillatory solutions were found. Millennial band oscillations were first found in OGCMs (Weaver et al. 1993; Winton and Sarachik 1993). Looking for a reduced model, Winton (1993) proposed a *three-box halocline oscillator*, which is special in the sense that the nonlinearity of the equation of state of seawater is crucial for the existence of the oscillations while unnecessary in the OGCMs. Further along, Sakai and Peltier (1999) built a three-degrees-of-freedom dynamical system using exclusively salinity variables and obtained regimes of oscillations that were used as prototypes for the Dansgaard–Oeschger millennial oscillations. Oscillations corresponding to spontaneous mode switching between thermal and haline states were observed by Zhang et al. (2002) to occur in a three-box model with a linear equation of state but using an advanced parameterization of convection. Recently Colin de Verdière et al. (2006, hereinafter CBS) used the simplest physical context to study millennial oscillations, namely a salt-conserving, hemispheric ocean basin, a linear equation of state for seawater, simple convective adjustment, linear dissipative dynamics, and time-independent mixed boundary conditions to show the existence of *windows of oscillations* in control space that depended on both the strength and the distribution of surface freshwater fluxes. Their simplest model that supported oscillations was found to be a 3 (horizontal) $\times$ 2 (vertical) box model in which the surface salinities and the deep temperatures played the crucial role. CBS's box model is similar to Huang et al.'s (1992) with the sole addition of diffusion. The first phase of the oscillations is well known from the early studies of Bryan (1986): a collapse of the THC occurs when the freshwater fluxes are strong enough. In the weak state of the THC, the deep layers warm by turbulent diffusion and for large enough warming, the surface halocline can break to allow convection to flux out the heat accumulated during the diffusive phase. The box model results confirmed by two-dimensional simulations showed further that the geographic distribution of the precipitation in polar regions was crucial to the existence of oscillatory regimes, and the suggestion was made that oscillations of the last glacial period might be due to the reduced precipitation rates found at that time. The window of oscillation regimes was found to be dependent on mixing processes, and the period observed in the models could accommodate easily the observed time scales of the last glacial period variability. A bifurcation similar to one of the bifurcations found by Cessi (1996) in the Welander model was found for the transition (oscillations $\rightarrow$ steady state, as the freshwater flux increases) characteristic of an infinite period, global bifurcation.

The 3×2 box CBS box model is an 11 ($=12 - 1$) degrees-of-freedom (because of salt conservation) dynamical system that is too complex for a theoretical analysis. The present paper originated from a desire to build a model of even lower hierarchy that should preserve the oscillatory character of the more complex model and at the same time allow a deeper physical understanding. Since a periodic oscillation requires only two degrees of freedom, the central question is, *which two variables are essential to describe millennial oscillations?* This paper proposes such a choice in section 2, provides a theoretical analysis of the model, and finds the boundaries of the bifurcations to oscillatory regimes as a function of freshwater flux (section 3). The simple oscillations that switch back and forth between a convective state and the haline fixed point of Stommel's model are studied in section 4 and may well be relevant to the physics of the millennial oscillations of glacial climate.

The reader may ask why such a simplified system is still studied today when increasing computing power allows one to reach these time scales with large-scale climate models. The answer to this legitimate question has been developed eloquently by Held (2005), who warns of the widening gap between comprehensive climate simulations and physical understanding and encourages the study of *model hierarchies* to narrow that gap. OGCM solutions depend on many parameterizations of subgrid-scale processes that are tested by comparisons with observations, here the large-scale property fields associated with the thermohaline circulation. However, since this circulation has not changed much over the last century, how can we be confident that the parameterizations found at steady state will also be adequate in transient regimes? The interest of the low-order model does not lie with the parameterizations but with the appropriate selection of critical large-scale processes. The possibility to map out easily the phase space of the solutions of such models against well-chosen control parameters may help to understand the

long-term sensitivity of the hierarchy of climate models. When structural similarity of bifurcation diagrams is found between a simple and a more complex system, there is indeed hope that the simple model captures the essential physics of the solutions.

Many important processes known to be important for the oscillations of the thermohaline circulation are neglected here. Wind forcing was shown to be important by Winton and Sarachik (1993): the circulation states of the oscillation are more realistic and the sensitivity to freshwater forcing changes. A complete mapping of the existence of the oscillatory regimes with respect to the wind amplitude remains to be carried out. Sea ice is also another important ingredient to consider given its effects on deep-water formation through brine rejection and its thermal insulation of the ocean interior. It has been shown by Loving and Vallis (2005) to play an essential role in a coupled model aiming at the conditions of the last glacial period. The objective of the present paper is to build up a model that elucidates the physics of a certain class of millennial oscillations. The choices are subjective and may be turned down when comparison with observations are made. On the other hand, the structure of such minimal models may help to analyze those higher up in the hierarchy. Borrowing again to Held (2005), we may expect that much will be learned when we observe how the dynamics change as these key sources of complexity are added.

2. The reduced THC model

The oscillations observed by CBS in models of various complexities give strong indications of the choices of model variables that have to be made. It is, indeed, suggested to the reader to browse through that paper to follow the simplifications made below. Since the oscillations are observed to be a process of episodic convection, the choice of a polar box model including a surface and a deep box is mandatory. These two boxes are then connected to midlatitude subpolar reservoirs with advection proportional to the horizontal pressure differences between the active polar box and the reservoir (Fig. 1). An extension of the Welander (1982) model in which a fixed rate of lateral exchange with a midlatitude reservoir was added was proposed by Lenderink and Haarsma (1994) to show the occurrence of convecting, nonconvecting, and periodic regimes with the possibility of multiple equilibria. Arzel (2004) used this model to explain certain aspects of the interdecadal oscillations that are found in OGCMs under mixed boundary conditions. The main differences with the Lenderink and Haarsma (1994) formulation are, first, that the temperature and salinity properties of the polar box can change the lateral transport rate with the reservoir and, second, that both the surface and the deep boxes are active.

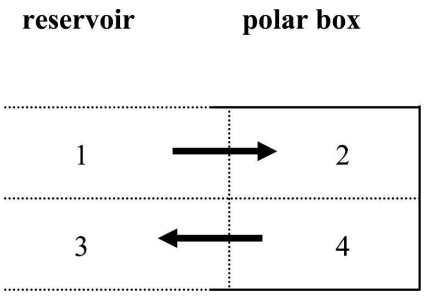

FIG. 1. Geometry of the active polar box. Overturning Ψ is positive when the flow is in the sense of the arrows. The circulation is then dominated by the effect of thermal anomalies.

To obtain an improved physical viewpoint, further simplifications are still needed. Among the four prognostic variables that remain, the surface temperature was chosen to be fixed on physical grounds. The surface heat flux is a strong negative feedback, which eliminates SST anomalies on monthly time scales (see Frankignoul et al. 1998). An objection to this put forward by Bretherton (1982) is that the strength of the feedback is bound to decrease as the scale of the anomaly increases. For global scales the damping of SST anomalies is controlled by the much weaker radiative cooling. Zhang et al. (1993) have shown that this lengthening of the relaxation time scale beyond about 200 days precludes the polar halocline catastrophe. The present formulation recognizes implicitly that the relaxation time scale has to be shorter than any other time scale involved in the millennial oscillation. Another obvious situation for which the surface temperature is fixed is that of a polar box covered by sea ice. But then sea ice has other effects that are not included here. When this hypothesis of constant surface temperature is made, one must bear in mind that the surface heat fluxes are nonzero and become *implicit*. When convection occurs, the deep temperature is set instantaneously to the value of the surface temperature and the associated heat loss is gained by the atmosphere. Although the surface temperature is "frozen," one must refrain from doing the same for the deep temperatures because the variation of the heat content of the deep layers caused by the successive phases of advection-/diffusion-dominated heat transport is one of the main signatures of the millennial oscillations observed in OGCMs. Quite remarkably nothing of the sort is observed for the salinities: deep anomalies are rather constant when anomalies at the surface may be one order of magnitude larger (see Fig. 9 in CBS). Although the heat con-

tent is free, the conservation of salt requires the surface integral of freshwater fluxes to vanish and the reduced amplitude of deep salinity anomalies is linked to the existence of this conservation law. Consider the phase of the oscillation when the THC is strong (thermally dominated). The salinity anomalies are small because the flow is fast. In the transition to the weak phase of the THC, the positive feedback between the flow and the salinity anomalies weakens the flow and the surface anomalies build up. Given the reduced exchange with the deep layers and the overall salt conservation, the deep layer salinities *are expected* to vary little during this phase. When the convection resumes, they decrease a little because of the destruction of the halocline but increase again because of the salinity–flow positive feedback working in reverse. However, if the decision is made that salinity is constant in the deep box, this choice must be considered ultimately an empirical one whose origin comes from the more comprehensive OGCM model results and is the main hypothesis of the paper. Of course, in this case salt is conserved only when the solution is at steady state. When it is periodic, the salt conservation again happens but only in an averaged sense (over a period). However, the nonconservation remains crucial at some points of the cycle.

Henceforth the reduced model, which is developed in what follows, is built up on the grounds that the two important variables to consider are *surface salinity and deep temperature*. Note that the pressure gradients, and hence the transport, between subpolar and polar boxes of Fig. 1 are not fixed because the polar surface and bottom densities vary. This configuration is close to the one put forward by Yin (1995) to explain interdecadal oscillations under mixed boundary conditions. Using surface temperature, surface salinity, and deep temperature as main prognostic variables, he describes interdecadal oscillations under mixed boundary conditions as flip–flop Welander-type oscillations. The circulation in Yin's model is represented by fixed transports (relaxation terms) as in Lenderink and Haarsma (1994). Although this choice may be accepted for the interdecadal oscillations that have small amplitudes, it is difficult to follow for the case of the large millennial oscillations.

To concentrate on the physics and be free of unnecessary complications, the two boxes (with index 2 at the surface and 4 at depth) are assumed of equal depth (mass) as this simplifies somewhat the analysis. With upstream differencing, the advection scheme depends on the sense of the circulation, and the equations obeyed by T_4 and S_2 are, respectively,

$$m\dot{T}_4 = \psi^+(T_2 - T_4) + \psi^-(T_4 - T_3) + D(T_3 - T_4) \tag{1a}$$

and

$$m\dot{S}_2 = p_2 + \psi^+(S_1 - S_2) + \psi^-(S_2 - S_4) + D(S_1 - S_2), \tag{1b}$$

where ψ is the mass transport between the reservoirs and boxes 2 and 4, D is the coefficient of lateral mixing, and p_2 is the freshwater forcing in box 2 (in this region of net precipitation p_2 is negative). The transport ψ is determined from a balance between friction and horizontal pressure gradients, and it relates to horizontal density differences between the active boxes and the reservoirs assuming hydrostatic pressure:

$$\psi = C[\alpha(T_1 - T_2) + \alpha(T_3 - T_4) - \beta(S_1 - S_2) - \beta(S_3 - S_4)]. \tag{2}$$

Here α and β are the coefficients of thermal and haline expansion, respectively, while ψ^+ and ψ^- are

$$\psi^+ = \frac{1}{2}(\psi + |\psi|) \quad \text{and} \quad \psi^- = \frac{1}{2}(\psi - |\psi|).$$

In this notation introduced by Thual and McWilliams (1992), ψ^+ is equal to ψ (and ψ^- is zero) when the circulation is positive (in the sense of Fig. 1), while ψ^- is equal to ψ (and ψ^+ is zero) when the circulation is negative. The reduced model has now only two prognostic variables, but this is at the expense of an increase in the number of control parameters. As it turns out, the physics of the problem becomes more transparent with variables other than T_4 and S_2. First change variables in favor of density variables x and y:

$$x = \alpha(T_4 - T_2) \quad \text{and}$$
$$y = \beta(S_4 - S_2).$$

After one chooses a scale $\tilde{\psi} = 10^9$ kg s^{-1} and a time scale $\tau = m/\tilde{\psi}$, (1a) and (1b) become

$$\dot{x} = -(\psi^+ - \psi^- + D)\,x + (D - \psi^-)\alpha\, T_{32} \quad \text{and} \tag{3a}$$

$$\dot{y} = -\beta p_2 - (\psi^+ - \psi^- + D)y - (D + \psi^+)\beta\, S_{14}, \tag{3b}$$

where D stands for $D/\tilde{\psi}$, p_2 stands for $p_2/\tilde{\psi}$, and T_{ij} stands for $T_i - T_j$ (with similar notations for S_{ij}). With these variables (2) becomes

$$\psi = C[\alpha(T_{12} + T_{32}) - \beta(S_{14} + S_{34}) - x - y], \tag{3c}$$

where C stands for $C/\tilde{\psi}$. Last, the variables x and y are exchanged in favor of the variables ψ and $\Delta\rho$, where $\Delta\rho$ is the stability of the column of the two active boxes, that is, $\Delta\rho = \rho_{\text{top}} - \rho_{\text{bottom}} = x - y$. The equations governing the rate of change of ψ and $\Delta\rho$ are obtained from (3a) and (3b), yielding

$$\dot{\Psi} = F - (\psi^+ - \psi^- + D)\,\psi + \psi_T\,\psi^+ - \psi_H\,\psi^- \quad (4a)$$

and

$$\dot{\Delta\rho} = G - (\psi^+ - \psi^- + D)\,\Delta\rho + r_2\,\psi^+ - r_3\,\psi^-, \quad (4b)$$

where $F = C(\beta p_2 + Dr_0)$, $\psi_T = C(r_1 + r_2)$, $\psi_H = C(r_1 - r_3)$, $G = \beta p_2 + D(r_2 + r_3)$, and the hydrology of the reservoirs appears through the parameters

$$r_0 = \alpha T_{12} - \beta S_{34},$$
$$r_1 = \alpha(T_{12} + T_{32}) - \beta(S_{14} + S_{34}),$$
$$r_2 = \beta S_{14}, \quad \text{and}$$
$$r_3 = \alpha T_{32}.$$

Only three of the r_i are independent since $r_1 + r_2 = r_0 + r_3$. The freshwater forcing p_2 is singled out as the primary control parameter, but there are others in addition to the r_i, namely C the inverse of a friction coefficient and D the coefficient of (lateral) diffusion. These last two are chosen from estimates of the present circulation. The main advantage of the present formulation lies in the fact that (4a) is independent of $\Delta\rho$, with consequences that solutions of this equation will be found to be identical with those of the Stommel (1961) model. This should not cause surprises since by (2) the overturning circulation is forced through horizontal density gradients and not vertical ones (the $\Delta\rho$ variable). Therefore the existence of fixed points of thermal or haline origin is expected. However the stability of such fixed points with respect to the dynamics, (4a), is not sufficient. The density equation in (4b) is coupled to the overturning both by the advection/diffusion terms but also through the last two terms, which will play an important role. This equation is valid only if the stratification is stable; therefore, a prescription for the unstable case must be added. Indeed, the addition of a degree of freedom in the vertical requires that the stability of the vertical column, $\Delta\rho \le 0$, be also satisfied if the Stommel's fixed points are to be reached. If in the course of the approach to a Stommel fixed point, the stability $\Delta\rho$ becomes positive, convection sets in, deep-water formation occurs, and mixing restores T_4 to T_2, S_2 to S_4, and $\Delta\rho$ to zero. Consequently x and y vanish and (3c) shows readily that the overturning ψ is *reset* to the convective value $\psi_c = C\,r_1$. The new aspect of the present model is then that ψ is coupled to $\Delta\rho$ whenever unstable convection sets in. To the two equations in (4), one must then add a third, which is the convective instability condition:

$$\text{If} \quad \Delta\rho > 0, \psi = \psi_C\,(=Cr_1). \quad (4c)$$

This condition can also be integrated in (4b) by adding a term $-H(\Delta\rho)\Delta\rho/\tau$, with H being the Heavyside step function and τ being an appropriate convective time scale very much smaller than 1. Note that the full dynamical system defined with (4a), (4b), and (4c) is nondifferentiable at $\psi = 0$ and $\Delta\rho = 0$. The latter is also shared by OGCMs when they do not resolve deep-water formation convection cells. The possible solutions to this system are now examined with freshwater forcing selected as the main control parameter.

3. The equilibrium solutions

a. The Stommel fixed points

Consider first the evolution of positive ψ as governed by the dynamics, (4a). Fixed points obey

$$(\psi^+)^2 + (D - \psi_T)\,\psi^+ - F = 0. \quad (5)$$

If the discriminant $\Delta_+ = (D - \psi_T)^2 + 4F$ is positive, two fixed points are expected (reducing to one when it is zero and none when it is negative). If $\Delta_+ \ge 0$, $\Psi_1^+ = \frac{1}{2}(\Psi_T - D + \Delta_+^{1/2})$ is one of the fixed points, and a perturbation ϕ (not necessarily small) is introduced as $\Psi^+ = \Psi_1^+ + \phi$ so that (4a) becomes

$$\dot{\phi} = -\Delta_+^{1/2}\phi - \phi^2. \quad (6)$$

Equation (6) is recognized as the normal form for a transcritical bifurcation but in the present case, the parameter Δ_+ cannot be negative and the bifurcation does not occur. The properties of (6) are readily obtained from the equation for the potential

$$V_+ = \frac{1}{2}\Delta_+^{1/2}\phi^2 + \frac{1}{3}\phi^3,$$

which allows us to rewrite (6) as

$$\dot{\phi} = -dV_+/d\phi$$

with the property that

$$\dot{V}_+ = -(dV_+/d\phi)^2 \le 0.$$

This demonstrates the finite-amplitude stability at the minima of V_+. There are two possibilities to consider: first since $V'' \ge 0$, $\phi_1 = 0$ is a minimum and is the well-known strong, thermally dominated branch of the Stommel model corresponding to Ψ_1^+. The other possibility, $\phi_2 = -\Delta_+^{1/2}$, is a maximum ($V'' < 0$) and corresponds to the second root of (6) and (5), $\Psi_2^+ = \frac{1}{2}(\Psi_T - D - \Delta_+^{1/2})$. Diffusion brings some differences with the Stommel model because positiveness (hence existence) of this second unstable root occurs only if $F < 0$; that is, for enough precipitation $|p_2| > Dr_0/\beta$, the parameter r_0 relates to the background meridional pressure gradient and is positive. The basin of attraction of these fixed points is the following:

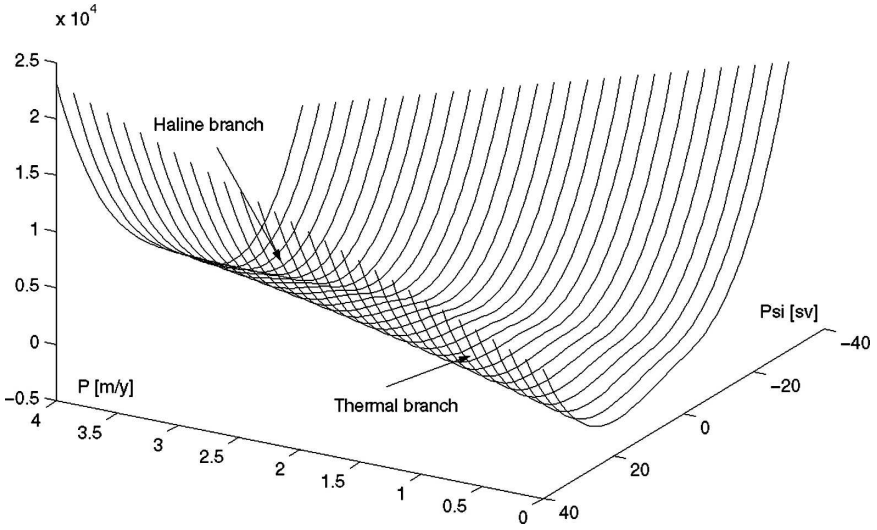

FIG. 2. The potential V as a function of the overturning and precipitation. The minima of the valleys are the position of the Stommel stable fixed points. When two valleys are present for the same value of the precipitation, the length of the ridge that separates them is the width of the hysteresis in the Stommel (1961) model.

- when $|p_2| < Dr_0/\beta$, all initial conditions are attracted to the stable fixed point Ψ_1^+;
- when $|p_2| = Dr_0/\beta$, all initial conditions are attracted to the stable fixed point Ψ_1^+ but $\Psi_2^+ = 0$ is neutral;
- when $Dr_0/\beta < |p_2| \leq (\Psi_T - D)^2/4C\beta - Dr_0/\beta$, all initial conditions for which Ψ^+ is larger (smaller) than Ψ_2^+ converge to Ψ_1^+ (0) [and what happens next is analyzed through (4b)];
- when $|p_2| > (\Psi_T - D)^2/4C\beta - Dr_0/\beta$, (i.e., beyond the saddle node bifurcation), all initial conditions lead to vanishing Ψ^+ and the further evolution must be analyzed with (4b).

Consider now the case of negative Ψ whose fixed points obey

$$(\psi^-)^2 - (D + \psi_H)\psi^- + F = 0. \tag{7}$$

When the discriminant $\Delta_- = (D + \psi_H)^2 - 4F$ is positive, $\Psi_1^- = \frac{1}{2}(\Psi_H + D - \Delta_-^{1/2})$ is the only fixed point. In terms of the perturbation ϕ to Ψ_1^-, (4b) becomes

$$\dot{\phi} = -\Delta_-^{1/2}\phi + \phi^2. \tag{8}$$

The only allowable fixed point is $\phi = 0$ and it is stable because the associated potential is minimum there. This is the weak haline fixed point of Stommel (1961) with basin of attraction as follows:

- when $|p_2| \leq Dr_0/\beta - (\Psi_H + D)^2/4C\beta$, there are no fixed point with $\Psi < 0$ and all initial conditions lead first to $\Psi^- = 0$ and then to the thermal fixed point Ψ_1^+;
- when $|p_2| > Dr_0/\beta - (\Psi_H + D)^2/4C\beta$, all initial conditions reach the stable haline fixed point Ψ_1^-.

An overall picture of the solutions of (4a) and (4b) is provided in Fig. 2 by the topography of the potentials V when the freshwater forcing varies with all other parameters kept fixed. Note in particular the ridge that separates the thermal and haline valleys when they exist. It is along this ridge that hysteresis can occur. With the present model, however, the picture is as yet incomplete because it is not known if the associated stratification is stable at the fixed points. We then proceed by examining (4b) and (4c).

b. *The stability of the stratification*

Suppose first that as Ψ moves toward the bottom of a valley in Fig. 2, the stratification remains stable; then its steady state value is either

$$\Delta\rho_1^+ = (r_2\Psi_1^+ + G)/(\Psi_1^+ + D)$$

for the thermal branch or

$$\Delta\rho_1^- = (-r_3\Psi_1^- + G)/(D - \Psi_1^-)$$

for the haline branch.

The Stommel fixed points are then nonconvecting and become fixed points of (4b) provided that

$$r_2\Psi_1^+ + G < 0 \tag{9a}$$

for the thermal branch

$$-r_3\Psi_1^- + G < 0 \tag{9b}$$

for the haline branch.

The analysis of the stability of the stratification of such states is straightforward since a perturbation $\delta\rho_o$ does not change the value of Ψ provided that (4c) does not occur. This will be the case for an infinitesimal perturbation. Then (4b) shows that $\Delta\rho$ is restored exponentially fast to its steady-state value and for the thermal branch, for instance,

$$\Delta\rho = \Delta\rho_1^+ + \delta\rho_o e^{-(\Psi_1^+ + D)t},$$

showing that the perturbation $\delta\rho_o$ is eliminated through an advective/diffusive time scale. If however a finite-amplitude perturbation occurs such that $\Delta\rho_1^+ + \delta\rho_o$ is positive, convective mixing via (4c) occurs to restore neutral conditions and then Ψ jumps to the convective value Ψ_C. What happens next depends on the sign of $\dot{\Delta}\rho$ near $\Delta\rho = 0$: if positive, convection persists and Ψ remains at Ψ_C while, if negative, the convective state is itself unstable. Therefore in addition to the three Stommel fixed points, (4b) and (4c) allow the existence of a fourth *convective* fixed point with $\Delta\rho = 0$ and $\Psi = \Psi_C$, which is stable if

$$r_2\Psi_C + G \geq 0. \tag{9c}$$

Note that the condition appropriate for positive Ψ has been used in (9c) because warmer temperatures in the subpolar box imply a positive hydrological parameter r_1 and a positive Ψ_C. This condition, (9c), completes the stability conditions (9a) and (9b) for the Stommel fixed points.

All of the figures are made with the box surface taken as a spherical sector of 45°–90° latitude and 60° longitude, equal depths of 2000 m, the streamfunction parameter $C = 1 \times 10^{-9}$ Sv (Sv $\equiv 10^6$ m^3 s^{-1}), $\alpha = 2 \times 10^{-4}$ °C^{-1}, $\beta = 0.8$, and diffusion $D = 2000$ W m^{-2} °C^{-1} unless stated otherwise in the captions. Figure 3 gives an example of the stability map of the four fixed points as a function of precipitation using modern values for the hydrological parameters r_i. For low values of precipitation, the dynamical system is attracted to the convective fixed point, as the thermal Stommel fixed point is convectively unstable. There is an exchange of stability between these two fixed points at point C since for higher precipitation the stratification of the thermal branch becomes stable. At point S, the saddle node bifurcation, the system is attracted to the haline Stommel fixed point. The latter is always stable, but note that, when the diffusion is taken into account, it exists only for large enough precipitation. The saddle node transition at S also occurs for higher precipitation, or the larger the diffusion. In a sense the diffusion is seen here to stabilize the thermal branch by requiring higher precipitation for the existence of (and transition to) the haline state. This sensitivity of the THC to diffusion has been discussed by Schmittner and Weaver (2000), who drew attention to the sensitivity of OGCMs' multiple climate states on ocean mixing. The effect of diffusion on Stommel's model has been discussed recently by Longworth et al. (2005) in the context of abrupt climate change.

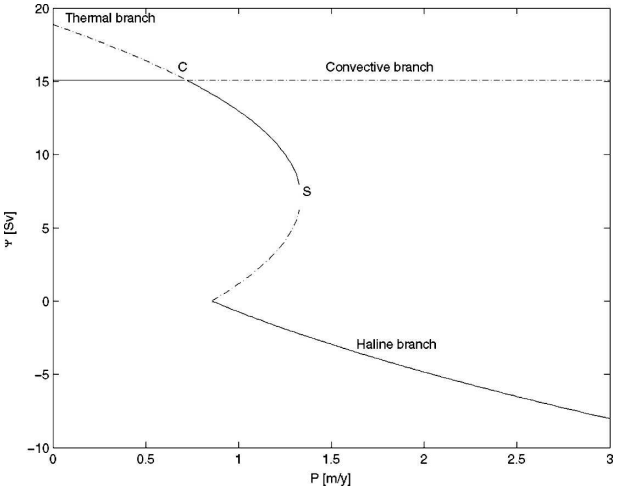

FIG. 3. The fixed points of the model as a function of the precipitation for a modern choice of the hydrological parameters r_i. Solid (dashed–dotted) lines indicate stability (instability) of the fixed point. For low values of P, the convective fixed point (horizontal line) is stable. It loses stability to the benefit of the Stommel thermal fixed point at point C. The latter has a stable stratification and exists up to the saddle node bifurcation at point S. The lower curve is the haline branch of the Stommel fixed point, which is always stable. This fixed point exists only beyond some threshold of the precipitation, an effect of the diffusion present in the model. (Parameters are as follows: $T_1 = 10$, $T_2 = 2$, $T_3 = 4$, $S_1 = 35.4$, $S_3 = 34.9$, and $S_4 = 34.9$.)

4. Thermohaline oscillations

The purpose of this simplified model is to identify easily the conditions for the existence of millennial thermohaline limit cycles. Because the system (4) is dissipative, the instability of fixed points leads necessarily to limit cycles, and two examples are considered below.

a. Implications of the thermal branch

Suppose first that precipitation is small, allowing the existence of the thermal Stommel fixed point, and that

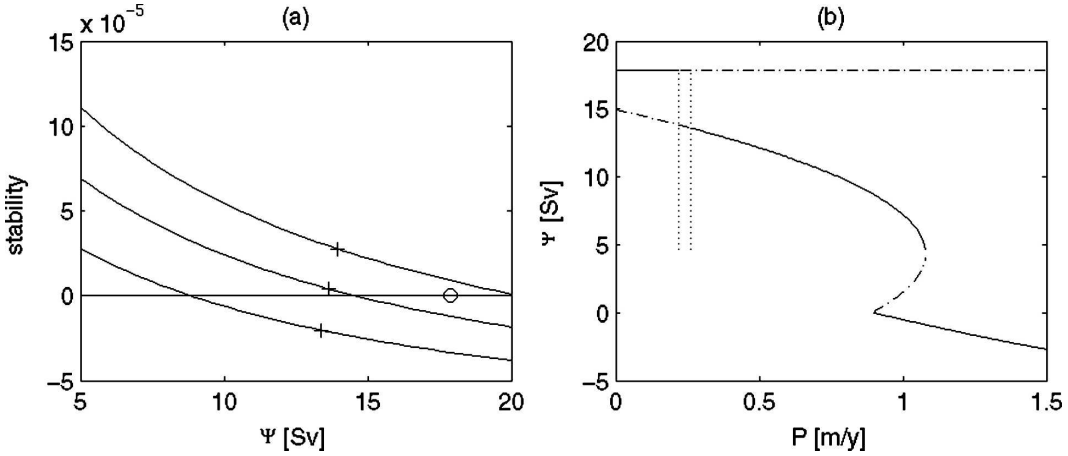

FIG. 4. Conditions for oscillations involving the thermal branch of Stommel model. (Parameters are as follows: $T_1 = 9$, $T_2 = 3$, $T_3 = 6$, $S_1 = 34.78$, $S_3 = 34.9$, $S_4 = 34.9$, and $D = 3500$ W m^{-2} °C^{-1}.) (a) The steady-state curves $\Delta\rho = f(\Psi)$ for three values of the precipitation 0.22, 0.24, and 0.26 m yr^{-1}. The convective fixed point is labeled by the open circle, and the three positions of the Stommel thermal fixed points are labeled by plus signs. Since oscillations require that both fixed points be unstable, the convective fixed point must be *above* the steady-state curve while the Stommel fixed point must be on the positive side of the $\Delta\rho$ axis. (b) The positions of the window of existence of the oscillation in the space Ψ vs precipitation as the two vertical dotted lines. Stable (unstable) fixed points are indicated by solid (dashed–dotted) curves. For less precipitation the convective steady state is stable and for more precipitation the Stommel fixed point is stable.

the overturning of the convective fixed point Ψ_C is larger than Ψ_1^+. Oscillations are expected if both fixed points are unstable. The convective fixed point is unstable if the buoyancy forcing is sufficient to induce a stable stratification, that is, a halocline just after convection. This requires that $\dot{\Delta}\rho < 0$ at $\Psi = \Psi_C$ and $\Delta\rho = 0$ or

$$r_2\Psi_C + G < 0. \tag{10a}$$

Similarly the instability of the Stommel fixed point requires that somewhere along the approach to Ψ_1^+, the stratification becomes unstable; therefore, a necessary condition is that

$$r_2\Psi_1^+ + G > 0. \tag{10b}$$

In this example r_2 must then be negative; that is, the surface salinity of the subpolar box must be less than the salinity of the deep layer. To find out the values of the control parameters allowing the two inequalities (10a) and (10b) to be satisfied, it is helpful to obtain from (4b) the steady-state relation that exists between $\Delta\rho$ and Ψ^+:

$$\Delta\rho(\Psi^+) = (r_2\Psi^+ + G)/(\Psi^+ + D).$$

This curve is plotted for three values of the precipitation in Fig. 4a. Instability requires that Ψ_1^+ be on the negative side of the $\Delta\rho$ axis and that Ψ_C be above the steady-state $\Delta\rho(\Psi^+)$ curve. From a state where the precipitation is low enough for the Stommel fixed point to be unstable, we see that increasing the precipitation further destabilizes the convective fixed point. When it is above the steady-state curve oscillations are expected. But, if the precipitation increases further, the stratification of the Stommel fixed point becomes stable. The window of the oscillatory solutions as a function of precipitation is shown in Fig. 4b. The window is very narrow and requires nonzero diffusion. The oscillations (not shown) are thermal in the sense that the forcing of the overturning is dominated by thermal gradients. Given the proximity of the convective and Stommel fixed points, the amplitude of the oscillations is not large. For a parameter regime typical of the present oceanic circulation interdecadal oscillations are obtained. The model solutions are likely to be similar to those of the fixed transport models of Lenderink and Haarsma (1994) and Yin (1995) and are not discussed further.

b. Implications of the haline branch

The same analysis can be made for the second case when the precipitation is so large that only the haline Stommel fixed point exists, that is, beyond the saddle node bifurcation *S* of Fig. 3. The condition of instability (10a) of the convective fixed point remains valid, but

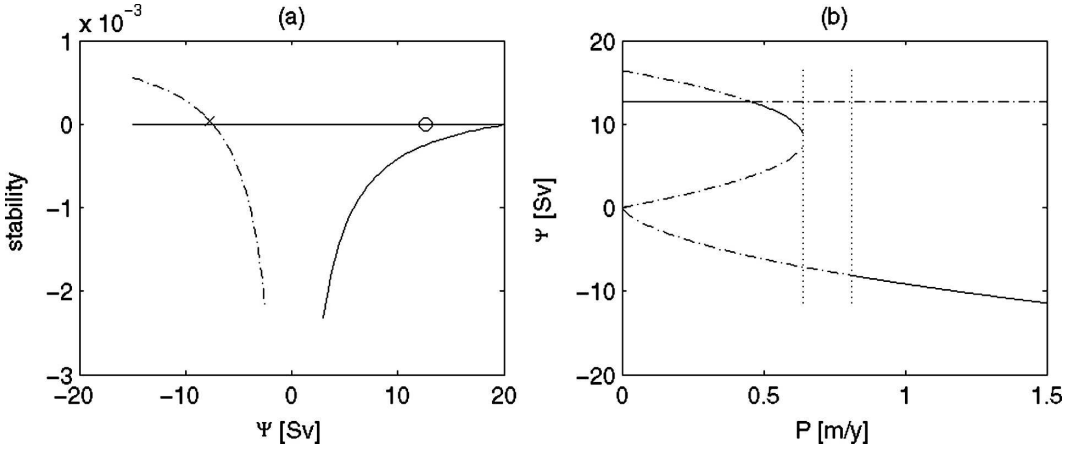

FIG. 5. Conditions for oscillations involving the haline branch of Stommel model. (Parameters are as follows: $T_1 = 9$, $T_2 = 3$, $T_3 = 8.5$, $S_1 = 35$, $S_3 = 35.2$, $S_4 = 34.9$, and $D = 0$.) (a) As in Fig. 4a but for an oscillation involving the haline branch of Stommel model. Note the change of shape of the $\Delta\rho = f(\Psi)$ curve for negative Ψ. (b) As in Fig. 4b but for a case where the oscillation window (the two dotted vertical lines) occurs for values of the precipitation beyond the saddle node bifurcation. To the left of this window the thermal nonconvecting Stommel branch is stable whereas to the right the haline nonconvecting Stommel branch is stable. In the window, the overturning oscillates between the convective regime and the haline Stommel branch.

the necessary instability condition of the haline Stommel fixed point requires, instead,

$$-r_3\Psi_1^- + G > 0. \tag{10c}$$

There are now two different branches for the steady-state $\Delta\rho(\Psi)$ curve, one for $\Psi > 0$ and one for $\Psi < 0$, as illustrated in Fig. 5. For high enough precipitation (beyond the saddle point), the Stommel fixed point and the convective fixed point are both unstable and oscillations occur. For still higher precipitation, the haline Stommel fixed point stabilizes. Note that the width of the window is much larger than in the previous case. This width can be shown to increase with an increase of T_3 and a decrease of S_4, two sensitivities which are easy to understand since both favor convection in the polar box. The situation of Fig. 5 was computed without diffusion. When diffusion is added, the window width increases but also moves to the right, requiring more precipitation for oscillations to occur.

These oscillations are now described for several cases respectively without and with diffusion. Figure 6 shows a case for a value of precipitation near the beginning end of the oscillation window of Fig. 5 and therefore close to the saddle node. Just after the onset of convection, the stratification builds up and the overturning decreases. At some point it slows down because it is close to the saddle node. After the slow passage in this "bottleneck," it speeds up to the haline fixed point. When this point is reached, the stratification decreases rapidly until convection resumes abruptly. Note the very different shape of the oscillations when precipitation and (or) diffusion moves the oscillation window away from the saddle node (Fig. 7): the overturning decreases regularly from the convective to the haline fixed point and slows down only in the vicinity of the haline fixed point. Note also that the stability variable $\Delta\rho$ is almost sinusoidal but for the cusp at $\Delta\rho = 0$. The last case that is shown in Fig. 8 corresponds to a precipitation value close to the second bifurcation (from the oscillatory to the steady haline state). In contrast to Fig. 7, note the long period taken for the stratification to become unstable. The tooth (comb) shape of the oscillations in Figs. 6 and 8 is typical of the behavior near the boundaries of the oscillation window. For values closer to the center of the window (Fig. 7), the oscillations lose this quasi-discontinuous character and are more regular. Note that in all three cases, the stratification becomes unstable as a result of the deep warming since the surface salinity is slightly decreasing in this approach to convection (see Figs. 6c, 7c, and 8c). These varieties of oscillations can be identified further by showing how the oscillation period depends on the precipitation. Figure 9 shows the period for the case without diffusion. Two infinite period bifurcations occur, one at the beginning end (the lowest precipitation value) and one at the far end of the oscillation window (the highest precipitation value), called first and second bifurcation in what follows. The first is characteristic of dynamical systems with saddle node bifurcations and

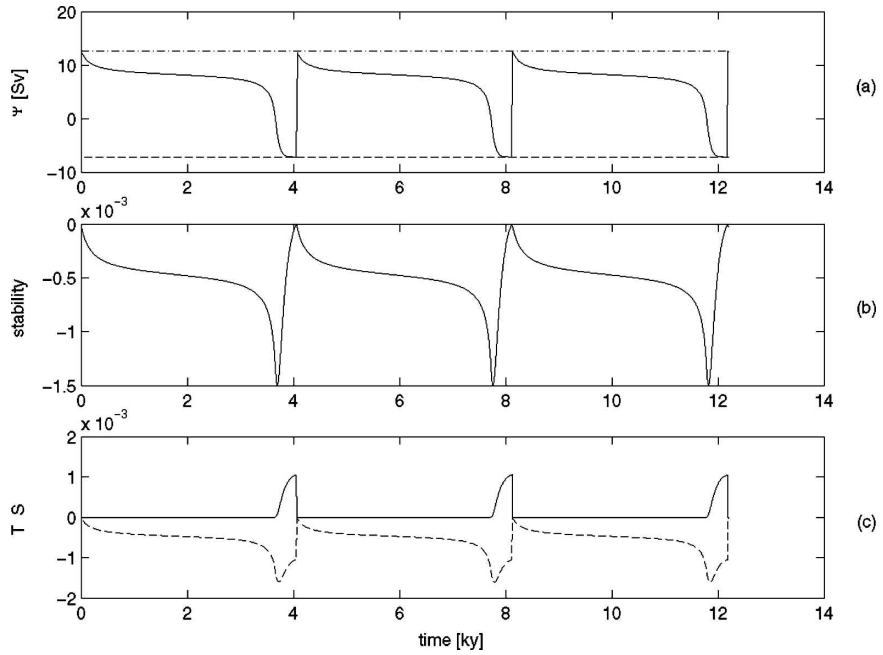

FIG. 6. Millennial oscillations involving the haline branch for the nondiffusive case and for a precipitation near the first bifurcation threshold. (a) The overturning Ψ and (b) the stratification stability $\Delta\rho$ are shown as a function of time. (c) The temperature T_4 and salinity S_2 in density variables $x = \alpha(T_4 - T_2)$ (solid) and $-y = \beta(S_2 - S_4)$ (dashed) so that convection occurs when $x = -y$. Note in particular the slowing of the overturning rate due to the presence of a ghost of the saddle node. The horizontal lines in (a) give the values of the convective and haline fixed points. (Parameters are as follows: $T_1 = 9$, $T_2 = 3$, $T_3 = 8.5$, $S_1 = 35$, $S_3 = 35.2$, $S_4 = 34.9$, $D = 0$, and $p_2 = 0.65$ m yr^{-1}.)

occurs in many branches of science. Strogatz's (1994) textbook describes the subject with the example of the overdamped pendulum described by the one-degree-of-freedom dynamical system on the circle $\dot{\theta} = \mu - \sin\theta$ (with θ being the angle of the rod, μ being the dissipation, and $\sin\theta$ being proportional to the torque of the weight). If $\mu < 1$, there are two fixed points θ_1 and θ_2 equal to $\sin^{-1}\mu$, and only the one with $0 < \theta < \pi/2$ is linearly stable. When $\mu_c = 1$, the two fixed points collide to make a half stable fixed point at $\pi/2$ through a saddle node bifurcation. When μ is larger than μ_c, however, there are no more fixed points and the motion is periodic. If μ approaches μ_c from above, the period becomes infinite and near this limit the period behaves as $(\mu - \mu_c)^{-1/2}$. To see the connection with the present model, consider (4a) with no diffusion and ψ positive:

$$\dot{\psi} = F - \psi^2 + \psi_T\psi. \tag{11}$$

After the change of variables $x = \frac{1}{2}\psi_T - \psi$, (11) becomes

$$\dot{x} = x^2 + \mu, \tag{12}$$

where $\mu = \psi_T^2/4 - F$. If $\mu = 0$, the overturning saddle node value is just $\frac{1}{2}\psi_T$. The bifurcation occurs when μ becomes positive. The important point is that when μ is very small, the solution can stay a very long time near $x \approx 0$ a state governed by the influence of the *ghost* of the nearby saddle node. If the period of the oscillations of the model equations in (4a)–(4c) is governed by what happens in this bottleneck, the period can be estimated asymptotically as

$$T \approx \int_{-\infty}^{\infty} \frac{dx}{\mu + x^2} = \pi/\sqrt{\mu}, \tag{13}$$

and Strogatz shows that this scaling of the period as an inverse square root of distance to bifurcation applies to the oscillations of the overdamped pendulum when μ is small. The slowing of the overturning in Fig. 6 is completely similar and the scaling, (13), is confirmed in Fig. 9. Now when diffusion is added, the first bifurcation occurs *away* from the saddle node, the "ghost" has a much reduced influence, and this process cannot occur. Figure 9 shows then that the period remains $O(1)$ at the transition of the first bifurcation.

The control at the second infinite-period bifurcation

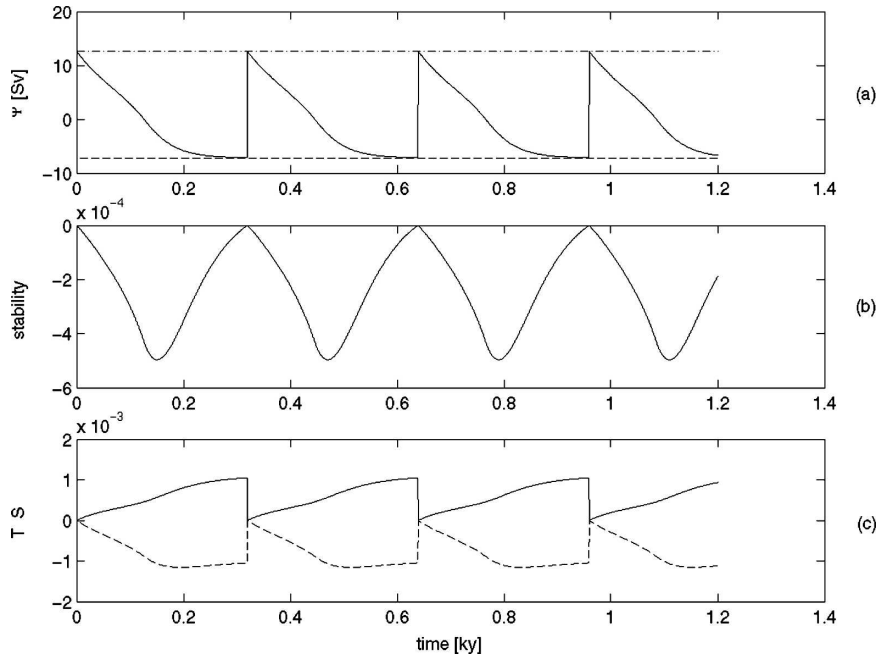

FIG. 7. Millennial oscillations involving the haline branch for the diffusive case for a precipitation in the middle of the oscillation window. Variables are shown as in Fig. 6. (Parameters are as follows: $T_1 = 9$, $T_2 = 3$, $T_3 = 8.5$, $S_1 = 35$, $S_3 = 35.2$, $S_4 = 34.9$, $D = 2000$ W m^{-2} °C^{-1}, and $p_2 = 1.25$ m yr^{-1}.)

(which is far from the saddle node) is different. Figure 8 shows that, when the overturning has reached the haline fixed point, there is a long waiting time before convection arises. This suggests that it is the time spent for the stratification to become unstable that is now the bottleneck of this infinite-period bifurcation. To explore this idea, (4b) near the haline fixed point ($\psi < 0$) reduces to

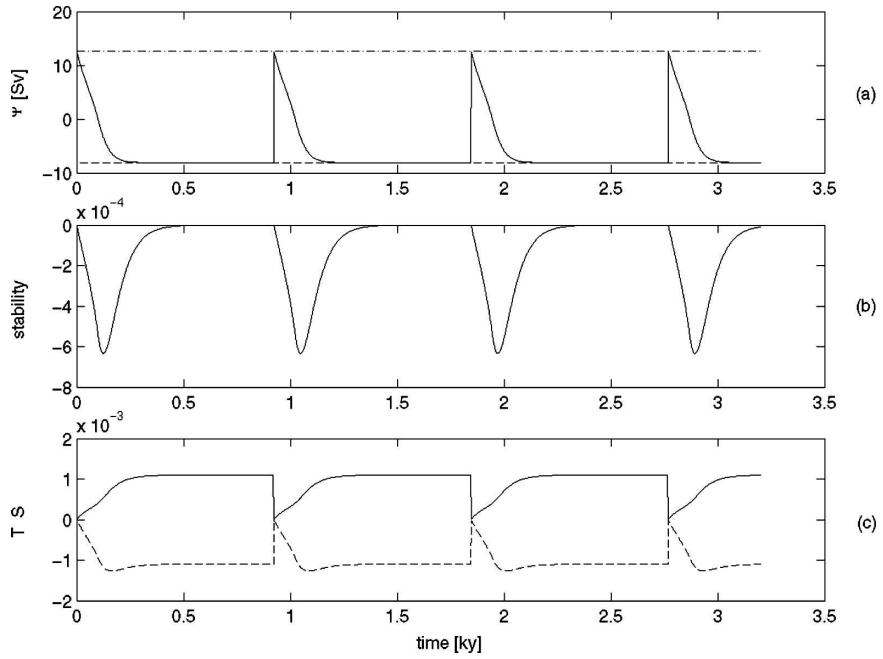

FIG. 8. As in Fig. 7, but near the second bifurcation threshold ($p_2 = 1.4479$ m yr^{-1}). Note the long waiting time needed for the stratification to become unstable.

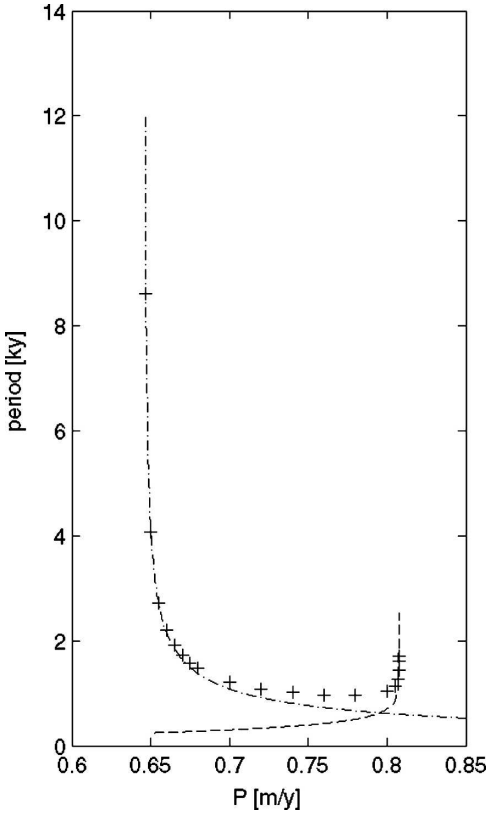

FIG. 9. The period of oscillation in the nondiffusive case as a function of the precipitation. The first (left) infinite-period bifurcation is captured by the dashed–dotted curve giving the inverse square root scaling typical of systems close to a saddle node. The dashed curve (for the second bifurcation) is the logarithmic scaling. (Parameters as in Fig. 6.)

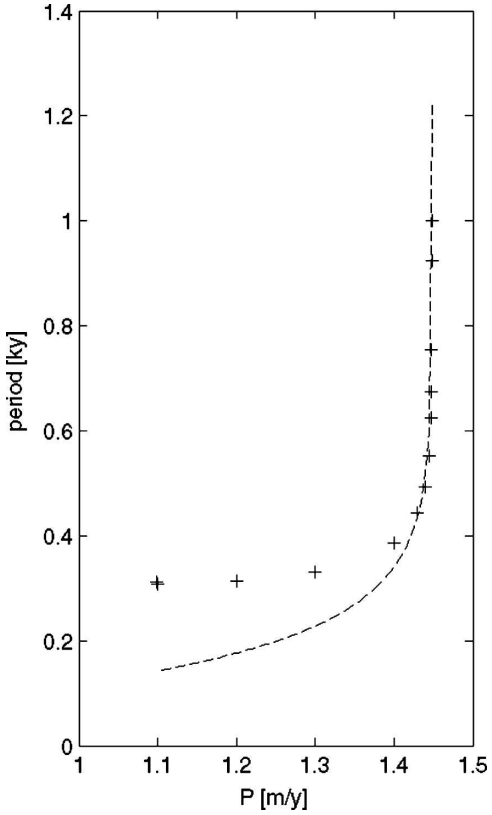

FIG. 10. The period of oscillation in the diffusive case as a function of the precipitation. The dashed curve (for the second bifurcation) is the logarithmic scaling. (Parameters as in Figs. 7 and 8.)

$$\dot{\Delta\rho} = G - (-\psi^- + D)\,\Delta\rho - r_3\psi^-. \tag{14}$$

Because ψ^- is nearly constant along this part of the cycle, (14) can be integrated locally as

$$\Delta\rho = [\Delta\rho_{\text{init}} - \mu/(-\psi^- + D)]e^{-(D-\Psi)t} + \mu/(-\psi^- + D), \tag{15}$$

where $\mu = G - r_3\psi^-$ is positive by the instability condition (10c). This phase of the cycle is interrupted when convection occurs at a time T given by $\Delta\rho = 0$ in (15). As μ goes to zero, the leading order term is $T \approx -\log\mu/(D - \Psi^-)$, and the asymptotic behavior of T (hence the period) varies as $\log(p_{2\text{critical}} - p_2)$ because μ varies linearly with p_2 over the range of interest. The argument applies with or without diffusion, and this logarithmic scaling for the second bifurcation has been indicated in Figs. 9 and 10. The difficulty of the test of this asymptotic law is caused by the restricted range of periods over which it can be tested with sufficient numerical accuracy.

5. Summary

The millennial oscillations described here have the nature of the flip–flop oscillations found by Welander (1982). Whereas Cessi (1996) argued for their importance for the interdecadal oscillations found in OGCMs, the present work argues similarly for the millennial oscillations but only once advective processes have been taken into account. Although Welander's oscillations occurred between *prescribed temperature–salinity reservoirs*, the present formulation permits oscillations to occur between *different circulation states*, a strong convective state and either of the Stommel states. In the context of the millennial oscillations, the most interesting case, however, involves the implication of the weak haline Stommel fixed point. Sufficient precipitation is needed for the system to operate beyond the saddle node bifurcation but not too much (!) because the haline Stommel fixed point recovers stability and the oscillations disappears. This is because the haline fixed point is destabilized by warming from below and stabilized by freshening from above. When operat-

ing near the saddle node (in the nondiffusive case), an infinite-period bifurcation is found with the familiar inverse square root scaling law for the period. Physically the solution is under the influence of a ghost of the saddle node, which slows down the system evolution. In the diffusive case, with freshwater forcing farther away from the saddle node, this cannot occur and the period remains $O(1)$ at the transition. The second bifurcation (oscillations $\rightarrow$ stable haline state as freshwater flux increases) is also of infinite period but of a different nature: it obeys a logarithmic dependency with distance to bifurcation, which is caused by the long time needed for sufficient warming of deep water to allow the onset of convection. The dependency of the period upon freshwater flux at the second bifurcation is identical to that found by Cessi (1996) for the Welander model. It is worth emphasizing that these bifurcations are global and are not Hopf bifurcations. Supercritical Hopf bifurcations have the properties of having infinitesimal amplitudes of the limit cycle at the bifurcation point, whereas periodic finite-amplitude migrations between two unstable fixed points are always observed in the present cases. Subcritical Hopf bifurcations do exhibit finite-amplitude limit cycles at a bifurcation point, but they also involve the joint presence of a steady fixed point, which is not a property of the dynamical system (4). Several aspects of these oscillations are found in the more complex two-dimensional model looked at by CBS: presence of the oscillations in a freshwater flux window, existence of the logarithmic infinite period for the second bifurcation, and the fact that the minimum of the oscillations is always close to the value of the nearby haline steady state. Absent in CBS, however, is the infinite-period character of the first bifurcation. It is conjectured that this may be due to the more diffusive regime of these solutions, which forces the oscillations to operate farther away from their saddle node equivalent. Indeed two-dimensional model simulations by F. Sévellec (2005, personal communication) and 3×2 box model exploratory calculations have shown that an abrupt infinite-period transition can also be found at the first bifurcation if smaller dissipation (hence stronger THC) is used. Quite clearly there is still work to be done to complete the geography of the phase space of these oscillations in the two-dimensional model.

Whether this type of oscillations is involved in (or explains part of) the millennial Dansgaard–Oeschger oscillations found in the last glacial period is an open question that requires careful and patient model–data comparisons. If glacial records of the oxygen isotopes over Greenland are interpreted in terms of atmospheric temperatures, the abrupt warming/slow cooling of the atmosphere revealed by these observations is captured by the present model of intermittent polar convection at millennial periods with its periodic heat flushes of the deep ocean to the atmosphere: as the deep ocean warms during the period of weak THC and interrupted convection, the needed heat is extracted from the atmosphere, which experiences a long cooling period. When the convection and THC resume, the deep ocean cools and the atmosphere experiences an abrupt warming. However, the identification of the important control parameters favorable to these oscillations at the time of the last glacial period remains a pressing question. In view of the importance given to the external forcing hypothesis of these paleo-oscillations (Alley et al. 2001; Ganopolski and Rahmstorf 2002; Braun et al. 2005), it is important not to forget this *other* hypothesis of self-sustained oscillations. Putting to the forefront the physics of *free oscillations* has often proved valuable in many geophysical problems because initial progress on the linearized problem was rapid. However the global bifurcations found here render the linear road unpractical: these ultralow-frequency oscillations have an intrinsic nonlinear character that makes them all the more interesting. A priority is to test their sensitivities to the variety of processes left aside purposely in the present study.

Acknowledgments. It is a pleasure to thank Olivier Marchal for comments on a first draft of this manuscript.

REFERENCES

Alley, R. B., P. U. Clark, L. D. Keigwin, and R. S. Webb, 1999: Making sense of millennial-scale climate change. *Mechanisms of Global Climate Change at Millennial Time Scales, Geophys. Monogr.,* Vol. 112, Amer. Geophys. Union, 385–394.

——, S. Anandakrishnan, and P. Jung, 2001: Stochastic resonance in the North Atlantic. *Paleoceanography,* **16,** 190–198.

Arzel, O., 2004: Mécanismes de variabilité climatique interdécennale dans des modèles idealisés. Ph.D. thesis, l'Université de Bretagne Occidentale, 242 pp.

Braun, H., M. Christl, S. Rahmstorf, A. Ganopolski, A. Mangini, C. Kubatzki, K. Roth, and B. Kromer, 2005: Possible solar origin of the 1470-year glacial climate cycle demonstrated in a coupled model. *Nature,* **438,** 208–211.

Bretherton, F. P., 1982: Ocean climate modeling. *Progress in Oceanography,* Vol. 11, Pergamon Press, 93–129.

Broecker, W., S. G. Bond, and M. Klas, 1990: A salt oscillator in the glacial Atlantic? I. The concept. *Paleoceanography,* **5,** 469–477.

Bryan, F., 1986: High latitude salinity effects and interhemispheric thermohaline circulation. *Nature,* **323,** 301–304.

Cessi, P., 1996: Convective adjustment and thermohaline excitability. *J. Phys. Oceanogr.,* **26,** 481–491.

Colin de Verdière, A., M. Ben Jelloul, and F. Sévellec, 2006: Bifurcation structure of thermohaline millennial oscillations. *J. Climate,* **19,** 5777–5795.

Dijkstra, H. A., and M. Ghil, 2005: Low-frequency variability of

the large-scale ocean circulation: A dynamical system approach. *Rev. Geophys.,* **43,** RG3002, doi:10.1029/2002RG000122.

Frankignoul, C., A. Czaja, and B. L'Heveder, 1998: Air–sea feedback in the North Atlantic and surface boundary conditions for ocean models. *J. Climate,* **11,** 2310–2324.

Ganopolski, A., and S. Rahmstorf, 2002: Abrupt glacial climate changes due to stochastic resonance. *Phys. Rev. Lett.,* **88,** 038501, doi:10.1103/PhysRevLett.88.038501.

Held, I. M., 2005: The gap between simulation and understanding in climate modeling. *Bull. Amer. Meteor. Soc.,* **86,** 1609–1614.

Huang, R. X., J. R. Luyten, and H. M. Stommel, 1992: Multiple equilibrium states in combined thermal and saline circulation. *J. Phys. Oceanogr.,* **22,** 231–246.

Lenderink, G., and R. J. Haarsma, 1994: Variability and multiple equilibria of the thermohaline circulation associated with deep-water formation. *J. Phys. Oceanogr.,* **24,** 1480–1493.

Longworth, H., J. Marotzke, and T. F. Stocker, 2005: Ocean gyres and abrupt change in the thermohaline circulation: A conceptual analysis. *J. Climate,* **18,** 2403–2416.

Loving, J. L., and G. K. Vallis, 2005: Mechanisms for climate variability during glacial and interglacial periods. *Paleoceanogaphy.,* **20,** PA4024, doi:10.1029/2004PA001113.

Ruddick, B., and L. Zhang, 1996: Qualitative behavior and nonoscillation of Stommel's thermohaline box model. *J. Climate,* **9,** 2768–2777.

Sakai, K., and W. R. Peltier, 1999: A dynamical system model of the Dansgaard–Oeschger oscillations and the origin of the Bond cycle. *J. Climate,* **12,** 2238–2255.

Schmittner, A. and A. J. Weaver, 2000: Dependence of multiple climate states on ocean mixing parameters. *Geophys. Res. Lett.,* **28,** 1027–1030.

Stommel, M. H., 1961: Thermohaline convection with two stable regimes of flow. *Tellus,* **13,** 224–230.

Strogatz, S. H., 1994: *Nonlinear Dynamics and Chaos with Applications to Physics, Biology, Chemistry and Engineering.* Advanced Book Program, Perseus Books, 498 pp.

Thual, O., and J. C. McWilliams, 1992: The catastrophe structure of thermohaline convection in a two-dimensional fluid model and a comparison with low-order box models. *Geophys. Astrophys. Fluid Dyn.,* **64,** 67–95.

Turner, J. S., 1973: *Buoyancy Effects in Fluids.* Cambridge University Press, 368 pp.

Velez-Belchi, P., A. Alvarez, P. Colet, and J. Tintore, 2001: Stochastic resonance in the thermohaline circulation. *Geophys. Res. Lett.,* **28,** 2053–2056.

Weaver, A. J., and T. M. C. Hughes, 1992: Stability and variability of the thermohaline circulation and its link to climate. *Trends Phys. Oceanogr.,* **1,** 15–70.

——, J. Marotzke, P. F. Cummins, and E. S. Sarachik, 1993: Stability and variability of the thermohaline circulation. *J. Phys. Oceanogr.,* **23,** 39–60.

Welander, P., 1982: A simple heat salt oscillator. *Dyn. Atmos. Oceans,* **6,** 233–242.

Winton, M., 1993: Deep decoupling oscillations of the oceanic thermohaline circulation. *Ice in the Climate System,* W. R. Peltier, Ed., NATO ASI Series, Vol. 112, Springer-Verlag, 417–432.

——, and E. S. Sarachik, 1993: Thermohaline oscillations induced by strong steady salinity forcing of ocean general circulation models. *J. Phys. Oceanogr.,* **23,** 1389–1410.

Yin, F. L., 1995: A mechanistic model of ocean interdecadal thermohaline oscillations. *J. Phys. Oceanogr.,* **25,** 3239–3246.

Zhang, R., M. Follows, and J. Marshall, 2002: Mechanisms of thermohaline mode switching with application to warm equable climates. *J. Climate,* **15,** 2056–2072.

Zhang, S., R. G. Greatbach, and C. A. Lin, 1993: A reexamination of the polar halocline catastrophe and implications for coupled ocean–atmosphere modeling. *J. Phys. Oceanogr.,* **23,** 287–299.